Correlation in thermal fluctuations induced by phase-locked hydrodynamic modes

Xiaohui Deng,[1] Xiaoping Wang,[2] and Ping Sheng[1,*]
[1]*Department of Physics, HKUST, Clear Water Bay, Kowloon, Hong Kong, China*
[2]*Department of Mathematics, HKUST, Clear Water Bay, Kowloon, Hong Kong, China*

(Received 29 November 2020; revised 29 April 2021; accepted 3 May 2021; published 18 May 2021)

Thermal fluctuations constitute a fundamental equilibrium phenomenon whose spatial and temporal correlations are governed by the relevant scales of molecular collisions. From the continuum point of view, thermal fluctuations in a fluid can be regarded as comprising a multitude of hydrodynamic modes (HMs) with random phases, each one having one degree of freedom. We show that in a two-dimensional fluid channel with the Navier slip boundary condition, in which the HMs are represented by periodic arrays of vortex and antivortex pairs, periodic modulation of the slip boundary condition can selectively suppress noncommensurate HMs while phase lock the remaining eigenmodes. As a result, thermal fluctuations would exhibit mesoscopic-scale spatial correlations, manifest as a spatially varying diffusion constant when evaluated from the fluctuation-dissipation theorem. Good agreement is shown with the molecular dynamics results. Such manifestation of equilibrium collective motion implies that instead of just being an alternative mathematical basis for expressing thermal fluctuations, in mesoscopic systems the HMs may be manipulated to have physical consequences very different from those expected in bulk fluid.

DOI: 10.1103/PhysRevE.103.053106

I. INTRODUCTION

Hydrodynamic modes (HMs) are the eigenfunctions of the Navier-Stokes (NS) equation under the appropriate boundary conditions. As the HMs are orthogonal to each other, in accordance to the equipartition theorem each one has one degree of freedom and therefore is activated by $\frac{1}{2}k_BT$ of energy in a thermal bath. Here k_B denotes the Boltzmann's constant and T is temperature. A HM represents a collective motion of the fluid, in sharp contrast to the Brownian motion of individual molecules. Therefore, in order to represent thermal fluctuations in terms of the HMs, one needs to reconcile the long-range correlations that exist in the HMs, with the very short-range spatial correlations that usually characterize the thermal fluctuations. In a previous publication [1], this reconciliation was accomplished by the addition of multiple HMs with random phases, thereby obliterating the long-range correlations of the HMs. In particular, in a two-dimensional (2D) mesoscopic channel the authors of Ref. [1] have shown the analytic solution of the HMs to comprise periodic arrays of vortex and antivortex pairs along both the axial channel direction (labeled x) and the height direction (labeled z). As the HMs can slide freely along the x direction, which can be represented by an added random phase in HM's periodic array, superposition of such HMs was shown to reproduce the thermal fluctuations time series with the same statistical properties as that obtained from molecular dynamics (MD). Through the orthogonality of the HMs, the fluctuation-dissipation theorem can also be expressed simply in terms of the eigenvalues of the HMs, and the resulting diffusion constant value was shown to be in good agreement with that obtained from molecular dynamics (MD) [1].

It is an intriguing question whether some traces of the HMs, with their long-range correlated fluid motion, can be observed in thermal equilibrium. If so, there can be important consequences since thermal fluctuations are fundamental to the statistical mechanics of equilibrium systems; any nonlocal correlations in thermal fluctuations would introduce new elements to the statistical ensemble averaging of physical parameters.

In this work, we show that by periodically modulating the slip length in the Navier boundary condition along the walls of a two-dimensional (2D) mesoscopic channel, the nonlocal correlations of phase-locked HMs can become partially detectable. This is due to the fact that the periodically modulated boundary condition can suppress those HMs with incommensurate periodicities, as well as add an energy cost to any movement (along the x direction) of the HMs that are commensurate with the periodicity of the boundary condition modulation. In this sense the relative phase of the periodic array of the HMs and that of the boundary modulation are "locked." We obtained good agreement between the theory prediction of nonlocal correlation and molecular dynamics (MD) simulations on the same system. In particular, we have observed mesoscopic-scale spatial correlations in equilibrium thermal fluctuations. Furthermore, diffusion along the x direction of the channel is shown to exhibit an unusual Einstein relation that corresponds to a spatially varying diffusion constant, consistent with the results on nonlocal correlations.

*sheng@ust.hk

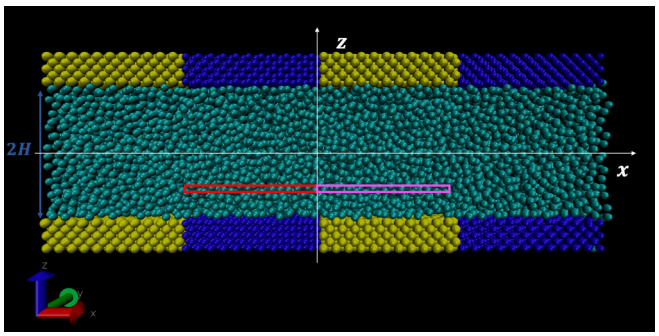

FIG. 1. A schematic illustration of the modulated boundary of a mesoscopic 2D channel with height $2H$ and width $2L$, with the fluid molecules at the equilibrium state. Yellow regions denote the segment where the solid wall-fluid intermolecular potential is given by $\delta_{wf} = 0.2$ in the notation of the Lennard-Jones potential, and blue regions denote the segment where solid wall–fluid intermolecular potential is given by $\delta_{wf} = 1.2$. The two red and pink rectangles denote the sampling regions for the evaluation of the velocity correlations.

II. SYSTEM GEOMETRY AND SOLUTION APPROACH

A. Geometry of the channel with modulated boundary condition

Consider a two-dimensional (2D) fluid channel with height $2H$ along the z direction and width $2L$ along the x direction. The center of the channel is located at $z = 0$. A schematic illustration of the fluid channel geometry is shown in Fig. 1, where the periodically modulated slip length $l_s(x)$ along the channel wall is delineated by different colored wall molecules.

While the geometry depicted in Fig. 1 is two dimensional, we suggest that such a system can be simulated approximately in three dimensions (3D) by using modulation stripes along the y direction. In such a system obviously dynamical anisotropy, e.g., in the diffusion constant, along the three orthogonal directions may be expected. However, in this work we intend to focus only on the nonlocal velocity correlation along the x direction and its associated implications.

B. Numerical solution of the HMs with modulated boundary condition

To obtain the HMs with periodically modulated boundary condition, we introduce the scalar potential $\phi(x, z, t)$ to represent the 2D velocity field $\vec{u}(x, z, t)$, and rewrite the hydrodynamic variables in anticipation of the exponential time-decay form,

$$u_x(x,z,t) = \frac{\partial\phi(x,z,t)}{\partial z}, \quad u_z(x,z,t) = -\frac{\partial\phi(x,z,t)}{\partial x}$$
$$\vec{u}(x,z,t) = \vec{u}(x,z)e^{-\lambda t}, \quad p(x,z,t) = p(x,z)e^{-\lambda t}. \quad (1)$$

The incompressible NS equation can be expressed in its eigenfunction form,

$$(\nabla^2 + \lambda R)\vec{u}(x,z) = \nabla p'(x,z), \quad (2)$$

where $R = \rho/\eta$, ρ is the fluid density, η the shear viscosity, $p'(x,z) = p(x,z)/\eta$, and λ denotes the eigenvalue which should be a positive real number characterizing the rate of decay. By taking the curl on both sides of Eq. (2), we eliminate the pressure field and obtain a biharmonic equation for the velocity scalar potential,

$$(\nabla^2 + \lambda R)\nabla^2\phi(x,z) = 0. \quad (3)$$

Equation (3) can be numerically solved by using the finite difference method with a fourth-order accurate central difference scheme. Numerical computations are based on LAPACK [2] and EIGEN [3] package libraries. Detailed procedures are given in Appendix A [4]. In Fig. 2 we give two examples of velocity eigenmodes with $l_s(x)$ given as

$$l_s(x) = \begin{cases} 1.5 & x \in [-32,-16)\bigcup[0,16) \\ 0.1 & x \in [-16,-0)\bigcup[16,32] \end{cases}, \quad (4)$$

where the scale of length is given in the Lennard-Jones unit σ used in MD simulations.

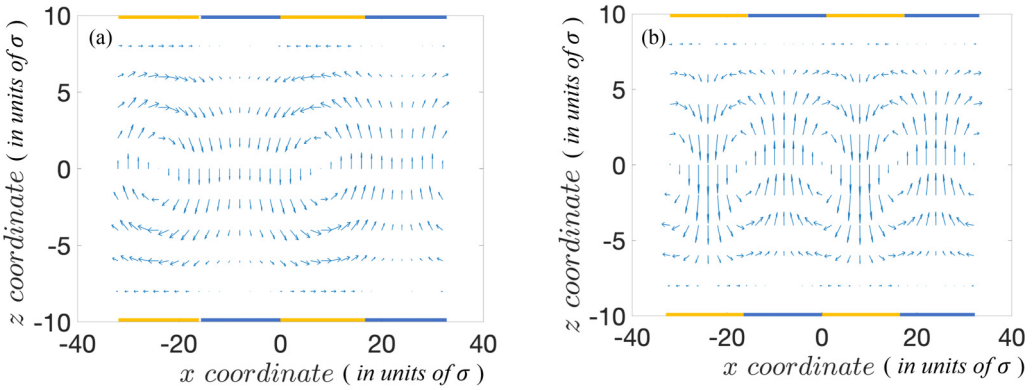

FIG. 2. Two velocity eigenmodes under the periodically modulated slip boundary condition with $L = 32$ and $H = 8$ in the Lennard-Jones length unit $\sigma = 0.34$ nm. Two different colors label the two different regions of slip length, as indicated in Fig. 1. (a) A plot of the velocity field for an eigenmode with $\lambda = 0.117$ in the Lennard-Jones unit of inverse time $\sqrt{\varepsilon/m\sigma^2}$, where ε is the energy unit and m is the mass unit. The length of the vector denotes the velocity magnitude. (b) A plot of the velocity field for an eigenmode with $\lambda = 0.132$. In both cases the modulated slip length is a piecewise constant function, given by Eq. (4). It is apparent that the velocity in the near-boundary region has a larger magnitude in the larger slip length segment (colored yellow).

C. Recapitulation of the approach for obtaining the slip length from MD

In the numerical solution approach described above, it is necessary to input the values of the slip length in the two regions of the periodic boundary condition modulation [5–8]. Since we would like to compare our theoretical results with those of MD simulations, there is a necessity for consistency between the two. Since our approach of getting the slip length from MD [1,9] differs from those better-known previous methods in the literature [10–12], here we briefly recapitulate our approach so as to make the present work more self-contained [1].

In order to obtain the two slip lengths as inputs to the numerical calculations, we use the analytical solution form (for the uniform boundary condition) obtained for the 2D channel [1] as the starting point, in which the slip length is a parameter in the solution form, appearing in the dispersion relation of the HMs:

$$\left(k_x^2 + k_z^2\right)\ell_s + k_x \tanh\left(k_x h\right) + k_z \tan\left(k_z h\right) = 0. \qquad (5)$$

Here k_x, k_z are the spatial wave vectors for the Fourier basis along the two directions; hyperbolic tangent and tangent functions are particular to the analytic solutions that are antisymmetric with respect to the center line of the channel, $z = 0$. Here $h < H$ denotes the position of the hydrodynamic boundary [6,7,9,13], which always exists implicitly in MD simulations, so that $2h$ denotes the domain of the HMs over which they must be orthogonal to each other. Also, it should be noted that $k_x^2 + k_z^2 = \lambda R$ for the analytic solutions of the HMs.

The approach for obtaining the two values of the slip length is simply to rely on the consistency between the ensemble-averaged MD simulation results with the solution of the NS equation. In order to get from Eq. (5) the slip length, the aim is to obtain from MD the values of k_z and h for a given value of k_x, so that ℓ_s can be directly solved from Eq. (5). How this can be achieved is briefly described below. As ℓ_s is a physical parameter, it should be independent of k_x, which has indeed been verified [1], so for simplicity we will use $k_x = 0$. Also, since we intend to use two different molecular interaction potential values between the solid and liquid in MD simulations, the above approach is to be used twice, so as to extract the two different slip length values from the MD simulations.

Since the parameters k_z and h are always implicit in MD simulations, to obtain them we first use the analytic form of the HM for a given set of (k_x, k_z) to project it onto an equilibrium configuration of MD, where k_x is always given *a priori* and k_z is treated as a continuously varying parameter. The projected configuration is then followed in time so as to evaluate its time correlation behavior. Invariably, an exponential decay was observed, and from the inverse of the slope a decay time can be obtained. Since only those discrete special values of k_z can satisfy the boundary condition, we expect that when the decay time is plotted as a function of k_z, at such values of k_z, that satisfy the boundary condition, the decay time should display a local maximum. This is expected from the fact that the Stokes equation can be derived from the principle of minimum energy dissipation [14]; hence any value of k_z that does not satisfy the boundary condition should display a faster decay, i.e., a shorter decay time. This indeed turned out to be true in practice. Once multiple k_z values are determined, the orthogonality property between any pairs of the analytic HMs can determine the value of h. This is easily done by integrating the product of two different HMs from $z = 0$ towards the solid boundary. Due to orthogonality, this integral invariably vanishes at a point some distance $h < H$ from $z = 0$. Surprisingly, the value of h for any two pairs of HMs determined in this manner is very consistent; i.e., h can be overdetermined [9].

III. MOLECULAR DYNAMICS SIMULATIONS

We would like to verify the observable spatial correlations by carrying out the MD simulations for a configuration-matched microfluid channel where its hydrodynamic parameters determined from MD trajectories are consistent with the hydrodynamic equations in the continuum limit [15–18]. We use GROMACS [19] to simulate a fluid with Lennard-Jones (LJ) potential [15,16] confined between two parallel solid walls. Detailed technical details of the MD simulations are given in Appendix B [4]. Here we give an overall view. The length unit $\sigma = 0.34$ nm, energy unit $\varepsilon = 0.997$ kJ/mol, and mass unit $m = 1.660 \times 10^{-27}$ kg were chosen as the reduced units of measurement. The equipartition theorem in our current system is fixed at $\langle \vec{v}_i \cdot \vec{v}_i \rangle = 0.201\varepsilon/m$ [16,20]. There are two types of atoms in the MD system, the fluid atoms and the solid wall atoms. The solid wall has three layers of atoms arranged in the face centered cubic (fcc) lattice, and the modulation of the slip boundary condition is achieved by interlacing two types of solid atoms in a piecewise manner along the wall. Both wall atoms interact with the fluid atoms via the LJ potential $u_{ij}(\vec{r}) = 4\varepsilon_{ij}[(\sigma_{ij}/r)^{12} - \delta_{ij}(\sigma_{ij}/r)^6]$ where *i,j* refer to either the fluid or the wall atom. Here "solid" is denoted by subscript w and "fluid" by subscript f. Since we have adopted the combination rule 1 for nonbonded interactions in GROMACS, their parameters have the corresponding relation with those in the LJ potential model given by $C_{12} = 4\varepsilon_{ij}\sigma_{ij}^{12}$ and $C_6 = 4\delta_{ij}\varepsilon_{ij}\sigma_{ij}^6$. The two different solid-fluid intermolecular potentials are distinguished by parameters $\delta_{wf}^{(k)}$, $k = 1, 2$. In MD simulations l_s and the precise position of the hydrodynamic boundary are implicit parameters, not known *a priori*. Our strategy is to first carry out the MD simulations on uniform slip length configurations and project the resulting (analytic) HMs of constant slip length onto MD trajectories with specified $\delta_{wf}^{(k)}$, $k = 1, 2$. As a result of the eigenmodes projection method [1], the hydrodynamic boundary position $h^{(k)}$ as well as the corresponding slip length $l_s^{(k)}$ can be uniquely determined and mapped to $\delta_{wf}^{(k)}$. Details of this approach are given in Appendix A [4]. In this manner and by interlacing two different constant fluid-solid intermolecular potentials along the x axis, we have implemented the hydrodynamic boundary condition of piecewise constant modulation of slip length $l_s(x)$. The channel's solid walls are divided into four different regions as shown in Fig. 1 and regions with the same color have exactly the same δ_{wf}. We list the relevant MD parameters as well as their corresponding slip length l_s in Table I.

TABLE I. The interaction parameters used in GROMACS. C_{12} and C_6 are the two coefficients of the nonbonded intermolecular potential model used for combination rule 1. Same basic units with GROMACS are used here.

	Case I	Case II
δ_{wf}	1.2	0.2
$C_{12}(\frac{\text{kJ}}{\text{mol nm}^{12}})$	Fluid-solid: 1.76750×10^{-5}	Fluid-solid: 1.76750×10^{-5}
	Fluid-fluid: 9.51704×10^{-6}	Fluid-fluid: 9.51704×10^{-6}
$C_6(\frac{\text{kJ}}{\text{mol nm}^6})$	Fluid-solid: 0.010851	Fluid-solid: 0.001808
	Fluid-fluid: 0.006161	Fluid-fluid: 0.006161
Slip length l_s (σ)	0.1	1.5

We have purposely chosen the two values of δ_{wf} that differ by a fairly large factor of 6, so as to accentuate the different slip length values in the two regions of the boundary condition modulation. These values were obtained by trial and error, after multiple tries. It can be seen that for the larger value of δ_{wf} the slip length is so small that it is essentially nonslipping.

IV. RESULTS

HMs reflect the properties of collective motions of moving fluid particles as a function of time t [21,22]. However, the collective motion behavior of the HMs cannot be manifest under the normal condition of uniform boundary conditions, since the translational symmetry along the x direction allows random phase additions as a function of time, leading to velocity correlations governed only by the scales of molecular collisions. In the present case, however, periodic modulation of the slip boundary condition can selectively phase lock the velocity eigenmodes by breaking their translational symmetry. Thus there can be dynamical correlations extending across the regions with different slip lengths. As a manifestation of such effect, thermal fluctuations should also exhibit mesoscopic-scale spatial correlations that are beyond the range of ballistic collisions. Below we show such manifestations from both the MD and HM perspectives, with good agreement between the two.

A. Mesoscopic correlation in the average absolute value of the velocity

Owing to the fact that the discretized matrices of both the Laplacian operator and biharmonic operator in Eq. (3) are real symmetric matrices, they admit orthonormal and complete basis functions set $\{\vec{u}_\beta\}$ which satisfies the relation

$$\sum_\beta \vec{u}_\beta(\vec{r})\vec{u}_\beta(\vec{r}') = \delta(\vec{r}-\vec{r}') \int |\vec{u}_\beta(\vec{r})|^2 d\vec{r}. \tag{6}$$

At any instant t the molecular velocity field $\vec{v}[\vec{r}_i(t)]$ can be expressed by superposing the continuum hydrodynamic velocity eigenmodes in terms of the eigenmode projection coefficient $A_\beta(t)$ via

$$A_\beta(t) = \frac{\sum_i^N \vec{v}[\vec{r}_i(t)] \cdot \vec{u}_\beta[\vec{r}_i(t)]}{\sum_i^N \vec{u}_\beta[\vec{r}_i(t)] \cdot \vec{u}_\beta[\vec{r}_i(t)]}, \tag{7a}$$

$$\vec{v}[\vec{r}_i(t)] \cong \sum_\beta^{\beta_{\max}} A_\beta(t)\vec{u}_\beta[\vec{r}_i(t)] \,, \tag{7b}$$

where $\vec{v}[\vec{r}_i(t)]$ denotes the velocity of the ith atom in MD simulations at position $\vec{r}_i(t)$ at time t, $\vec{u}_\beta[\vec{r}_i(t)]$ denotes the velocity of the βth eigenmode at position $\vec{r}_i(t)$, and N is the total number of fluid atoms. The maximum eigenmode index $\beta_{\max}$ corresponds to the minimum decay time required for the molecular collisions to establish the diffusive behavior. The value of this minimum decay time can be established from MD simulations by plotting the mean square displacement versus t, in which there is inevitably a quadratic region, indicating ballistic behavior, before entering the linear diffusive regime [16,21–23].

On the right-hand side of Eq. (7b) we have an additive sum of the velocity eigenmodes, each one of which displays mesoscopic velocity correlations inherent in the collective motion of the fluid. It is a legitimate expectation to see if $\vec{v}[\vec{r}_i(t)]$ can display some trace of such nonlocal correlations.

To see explicitly whether such nonlocal correlations exist, we employ MD simulations to evaluate the time series in the difference in velocity squared—$d(t) := \langle v_r^2 - v_l^2 \rangle_{\text{spatial}}(t)$. Here v_l^2 denotes the velocity squared of the molecules located inside the left-hand side sampling region shown in Fig. 1, colored red, and v_r^2 denotes the velocity squared of the molecules located inside the sampling region located inside the right-hand side sampling region that is colored pink. Two cases were examined—one with the periodic modulation of the boundary condition and the other one with the uniform boundary condition. To smooth the large oscillations in the time series $d(t)$, we used a moving time window of length $N_w = 1000$ time steps to average out the fluctuations. The results are shown in Fig. 3(a) for the case where the slip boundary condition is uniform, i.e., no modulations. The red curve denotes the window-averaged velocity square difference. The value of $\langle d(t) \rangle$ is close to zero as expected. Here the error bar is obtained by evaluating 4000 different time series, each with a relatively short duration to obtain the variance from the mean. Figure 3(b) shows the same results for the case when the boundary condition is periodically modulated, as shown in Fig. 1 with the parameters given in Table I. There is clearly a nonzero correlation over mesoscopic scales. This comparison clearly indicates the existence of partially detectable nonlocal correlations in the average absolute value of the velocity field in the case of the modulated boundary condition.

B. Spatially varying diffusion constant

As pointed out by Onsager [24], the time correlation of equilibrium fluctuations is governed by the same transport

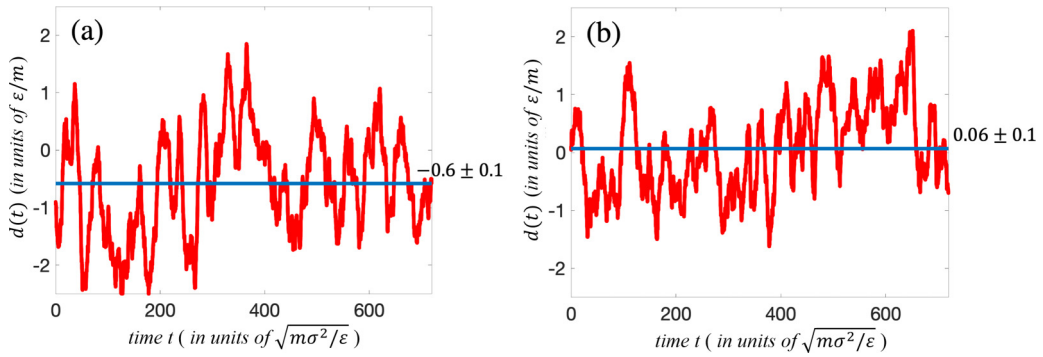

FIG. 3. (a) Difference in the square of the velocity in two slip regions shown in Fig. 1, $\langle v_l^2 - v_r^2 \rangle_{\text{spatial}}(t)$, plotted as a function of time t. The red curve represents the result from the moving window averaged over 1000 time steps. (a) In the uniform hydrodynamic boundary case the mean value is close to 0 as expected. The mean value is labeled by the blue straight line. (b) In the modulated hydrodynamic boundary case there is a clear nonzero collective correlation between the fluid motions over mesoscopic separations.

coefficient, e.g., the viscosity, as that governing the relaxation process exhibited by the solution of the NS equation. One of its representative dynamic implications is the diffusion constant D which describes the ratio between the diffusive flux and its local concentration gradient. According to the Kubo formula [25,26],

$$D = \frac{1}{2}\int_0^\infty \langle \vec{v}_i(0)\cdot\vec{v}_i(\tau)\rangle d\tau. \tag{8}$$

Equation (8) can be expressed in terms of the HMs by using Eq. (7). By invoking the equipartition theorem for each eigenmode as an independent degree of freedom, we obtain the diffusion constant distribution as

$$\begin{aligned} D(x,z) &= \frac{1}{2}\int_0^\infty \left\langle \sum_\beta \sum_\alpha A_\beta(0)A_\alpha(\tau)\vec{u}_\beta(0)\cdot\vec{u}_\alpha(\tau)\right\rangle d\tau \\ &= \frac{1}{2}\sum_\beta^{\beta_{\max}} \frac{1}{\lambda_\beta}\langle A_\beta^2(0)\rangle |\vec{v}_\beta(x,z)|^2 \\ &= \frac{1}{2}\frac{k_BT}{\rho}\sum_\beta^{\beta_{\max}} \frac{1}{\lambda_\beta}\frac{1}{\int\left[u_{\beta,x}^2(x,z)+u_{\beta,z}^2(x,z)\right]dxdz}|\vec{u}_\beta(x,z)|^2. \end{aligned} \tag{9}$$

From Eq. (9) it is clear that even when the system is under the same temperature, there can still be nonlocal spatial correlations introduced by the HMs as shown by Fig. 3. In other words, the usual kinetic theory has to be modified in this case; instead of each molecule having a fixed amount of thermal kinetic energy, now the spatial unit of accounting should be the HM.

By focusing on the statistical spatial correlations along the x direction, we spatially average with respect to z:

$$D(x) = \frac{1}{2H}\int D(x,z)dz \approx \frac{1}{N_s}\sum_k D(x,z_k). \tag{10}$$

From Fig. 1, it is expected that $D(x)$ may exhibit spatial variations on the mesoscopic scale that is commensurate with the periodic modulation of the boundary condition; i.e., the collective motions of the HMs should be partially manifest in both thermal fluctuations as well as the diffusion constant.

To measure the local diffusion constant in the MD simulation so as to compare with that evaluated from Eq. (10), we simply plot the square of displacement versus time and measure half the slope of the straight line region [16]. The displacement is within a single region of the slip boundary condition, which is done by choosing an appropriately large-sized box at different positions along the x axis as our monitoring window, and limit the time interval to be small enough so that the measured atom within the box does not drift out. To perform the average along the z axis as shown in Eq. (9), we choose $z = 0,\ 3.0,\ 6.0,\ 6.9\,\sigma$ as the four starting positions and carry out the Einstein relation measurements. Then $D(x)$ is obtained by averaging the four measured values.

To compare the region-averaged diffusion constant D computed by HM superpositions, i.e., Eq. (10), with that evaluated from MD simulations by using the Einstein relation, we plot the diffusion constant as evaluated from the HM data points as blue lines in Fig. 4 and the MD results as red dots. Good consistency can be seen, in which the spatial variations along the x direction reveal that the hydrodynamic boundary modulation has indeed led to observable consequences beyond the

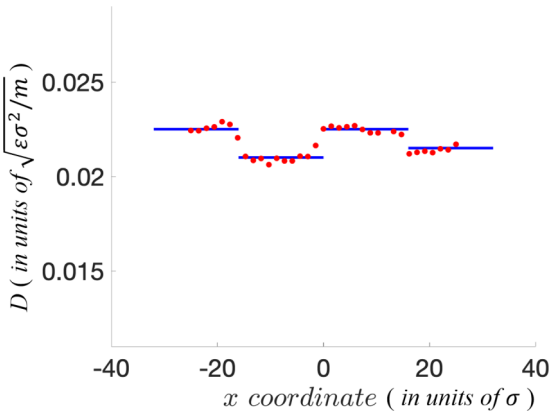

FIG. 4. Comparison of region-averaged diffusion constant D calculated by HM superposition (blue lines) and data points measured from MD trajectories (red dots). There is ∼5% relative error between the two results.

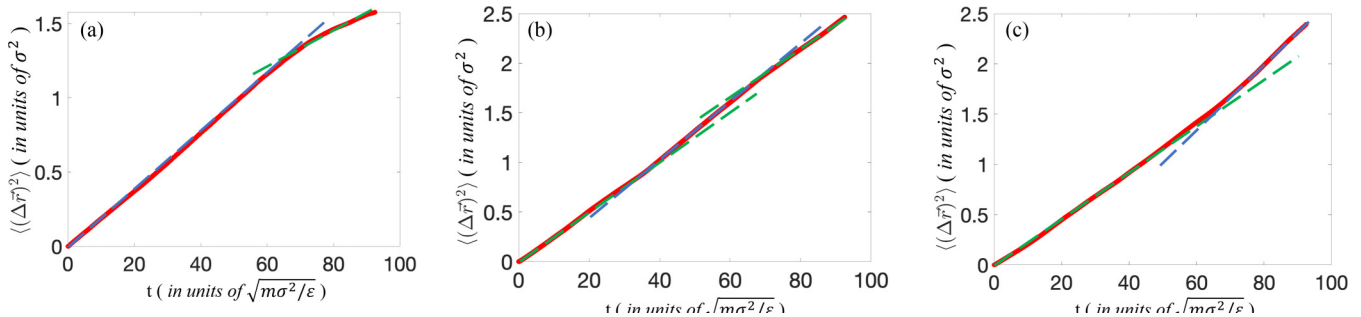

FIG. 5. A schematic plot of three different representative Einstein relations under the modulated boundary conditions. (a) A small group of fluid particles, i.e., one or two which are located in the region $x \in [-L, -L/2]$, are monitored for their long-time diffusion behavior. It is seen that at first the Einstein linear relation holds, but later an apparent drop in slope can be seen as it drifts into the neighboring region in which the diffusion constant is smaller. (b) A case where a small group of fluid particles is selected in the region $x \in [-L/2, 0]$ and the mean square displacement curve retains a near-constant asymptotic slope. (c) Contrary to case (a), an apparent rise in slope is seen after the particles drift into a neighboring region in which the diffusion constant is larger.

molecular collision length scale. In view of velocity eigenmodes, it is not surprising that the mobility within the larger slip length region is larger than that of the neighboring regions, hence a slightly larger diffusion constant.

C. Einstein relation

As a manifestation of the different diffusion constant values in different spatial regions, the dynamic behavior of the fluid particles as evaluated by the mean squared displacement $\langle(\Delta x)^2\rangle$ as function of t should exhibit nonlinear asymptotic behavior when t is large enough so that the particle can drift into different modulated regions. Figure 5 presents three different representative Einstein relations under the modulated boundary conditions. Due to the different mobilities in different regions and depending on whether the fluid atoms drift into the region with a larger or smaller diffusion constant, the tail part of the displacement curve can display a larger or smaller asymptotic slope, as delineated in Fig. 5 by straight dashed lines. Of course there is the possibility of the fluid particles staying within one region for a long time, so that the linear asymptotic slope can be maintained over the measurement timescale as shown in Fig. 5(b).

V. SUMMARY

To recapitulate, we show that with the modulated slip boundary condition in a mesoscopic fluid channel, there can be spatial correlations in thermal fluctuations that extend beyond the microscopic ballistic collision scales. This is due to the breakdown of translational symmetry by the periodic modulations of the slip boundary condition along the channel's walls, leading to phase locking of the HMs. We demonstrate the existence of mesoscopic-scale spatial correlations by using MD simulations, which show good agreement with the predictions of the phase-locked HMs through the fluctuation-dissipation theorem.

ACKNOWLEDGMENT

P.S. wishes to acknowledge the support of Research Grants Council of Hong Kong Grant No. 16303918.

APPENDIX A

Here we present the detailed numerical procedures of computing the eigenfunctions of the biharmonic equation of the scalar potential $\phi(x, z)$,

$$(\nabla^2 + \lambda R)\nabla^2\phi(x, z) = 0. \tag{A1}$$

The rectangular channel is discretized by an evenly distributed mesh with N_x grid points along the x direction and N_z grid points along the z direction. Integer pairs (i, j) are used to index the grid points of the function $\phi(x, z)$ at positions $-L + (i-1)\Delta x$, $-H + (j-1)\Delta z$ where i denotes the index along the x axis and j denotes the index along the z axis, shown in Fig. 6. By using this notation, the biharmonic differential operator can be discretized by using the finite difference method (FDM) with a fourth-order accuracy central difference scheme as [27]

$$\begin{aligned}
\nabla^2\nabla^2\phi &= \frac{\partial^4\phi}{\partial x^4} + 2\frac{\partial^4\phi}{\partial x^2\partial z^2} + \frac{\partial^4\phi}{\partial z^4} \\
&= \frac{1}{(\Delta x)^4}\phi_{i-2,j} - \left[\frac{4}{(\Delta x)^4} + \frac{4}{(\Delta x)^2(\Delta z)^2}\right]\phi_{i-1,j} \\
&\quad + \left[\frac{6}{(\Delta z)^4} + \frac{6}{(\Delta x)^4} + \frac{8}{(\Delta x)^2(\Delta z)^2}\right]\phi_{i,j} \\
&\quad - \left[\frac{4}{(\Delta x)^4} + \frac{4}{(\Delta x)^2(\Delta z)^2}\right]\phi_{i+1,j} + \frac{1}{(\Delta x)^4}\phi_{i+2,j} \\
&\quad + \frac{1}{(\Delta z)^4}\phi_{i,j-2} - \left[\frac{4}{(\Delta z)^4} + \frac{4}{(\Delta x)^2(\Delta z)^2}\right]\phi_{i,j-1} \\
&\quad - \left[\frac{4}{(\Delta z)^4} + \frac{4}{(\Delta x)^2(\Delta z)^2}\right]\phi_{i,j+1} + \frac{1}{(\Delta z)^4}\phi_{i,j+2} \\
&\quad + \frac{2}{(\Delta x)^2(\Delta z)^2}(\phi_{i-1,j+1} + \phi_{i+1,j+1} \\
&\quad + \phi_{i-1,j-1} + \phi_{i+1,j-1}),
\end{aligned} \tag{A2}$$

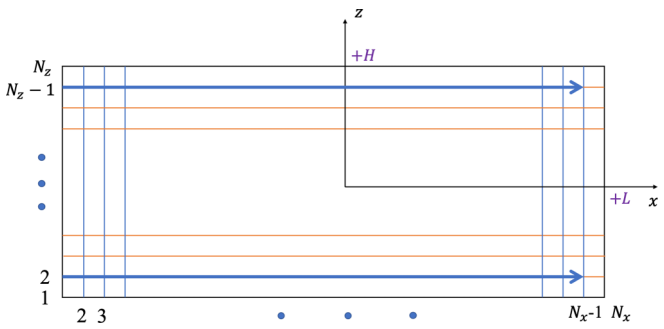

FIG. 6. A schematic representation of the uniformly discretized mesh. Here $i = 1$ and $i = N_x$ correspond to the left and right sides of the hydrodynamic boundary $x = -L$, $x = L$, respectively, while $j = 1$ and $j = N_z$ correspond to the lower and upper hydrodynamic boundary $z = -H$, $z = H$, respectively. Blue arrows indicate the natural index sequence when assembling the eigenmode vectors $\hat{\boldsymbol{\phi}}$ as well as the coefficient matrix $\boldsymbol{L}$ and $\boldsymbol{B}$. From the Navier slip boundary condition $u_z(x, \pm H) = 0$, stream function $\phi(x, z)$ should be constant at grid points $(i, 1)$, (i, N_z), while the equality $\phi_{1,j} = \phi_{N_x,j}$ holds at the hydrodynamic boundary at $x = \pm L$ owing to the periodicity of the boundary condition along the x axis. Therefore the grid points for the unknown values of $\phi(x, z)$ only cover the set $\{\phi_{i,j} | i = 1, 2, \ldots, N_x - 1,\ j = 2, 3, \ldots, N_z - 1\}$ which we denote as the "interior points." The "interior points" are to be solved from the discretized matrix equations.

and the Laplacian operator can be discretized as

$$\begin{aligned}\left(\nabla^2\phi\right)_{i,j} &= \frac{\partial^2\phi}{\partial x^2} + \frac{\partial^2\phi}{\partial z^2} \\ &= -\frac{1}{12}\frac{1}{(\Delta x)^2}\phi_{i-2,j} + \frac{16}{12}\frac{1}{(\Delta x)^2}\phi_{i-1,j} \\ &\quad - \frac{30}{12}\left[\frac{1}{(\Delta x)^2} + \frac{1}{(\Delta z)^2}\right]\phi_{i,j} + \frac{16}{12}\frac{1}{(\Delta x)^2}\phi_{i+1,j} \\ &\quad - \frac{1}{12}\frac{1}{(\Delta x)^2}\phi_{i+2,j} - \frac{1}{12}\frac{1}{(\Delta x)^2}\phi_{i,j-2} \\ &\quad + \frac{16}{12}\frac{1}{(\Delta x)^2}\phi_{i,j-1} + \frac{16}{12}\frac{1}{(\Delta x)^2}\phi_{i,j+1} \\ &\quad - \frac{1}{12}\frac{1}{(\Delta x)^2}\phi_{i,j+2}. \end{aligned} \tag{A3}$$

For simplicity the Navier slip boundary condition is discretized by using the second-order accuracy central difference scheme as

$$\begin{aligned} l_s[i]\frac{\phi_{i,2} - 2\phi_{i,1} + \phi_{i,0}}{(\Delta z)^2} &= \frac{\phi_{i,2} - \phi_{i,0}}{2\Delta z}, \\ l_s[i]\frac{\phi_{i,N_z+1} - 2\phi_{i,N_z} + \phi_{i,N_z-1}}{(\Delta z)^2} &= -\frac{\phi_{i,N_z+1} - \phi_{i,N_z-1}}{2\Delta z}, \\ \phi_{i,1} &= \phi_{i,N_z} = 0, \end{aligned} \tag{A4}$$

from which we can express the ghost points in terms of the interior points:

$$\phi_{i,0} = \frac{\Delta z - 2l_s[i]}{\Delta z + 2l_s[i]}\phi_{i,2}, \quad \phi_{i,N_z+1} = \frac{\Delta z - 2l_s[i]}{\Delta z + 2l_s[i]}\phi_{i,N_z-1}, \tag{A5}$$

where $l_s[i]$ denotes the value of the slip length $l_s(x)$ at grid points $-L + (i-1)\Delta x$, 1 and $-L + (i-1)\Delta x$, N_z. In this manner, we transform the differential operator $\nabla^2\nabla^2$ and ∇^2 to the discretized coefficient matrices $\mathbf{B}$ and $\mathbf{L}$, respectively, from which we would like to obtain the eigenvectors of $\mathbf{B}\widehat{\phi} = -\lambda R\mathbf{L}\widehat{\phi}$. A schematic illustration of the solution procedures is listed in the flow chart, Fig. 7, where the arrows indicate the flow sequence. Our basic strategy is to transform the generalized eigenvector problem to the standard eigenvalue problem form $\mathbf{A}\widehat{x} = \lambda\widehat{x}$. Here the constant $R = \rho/\eta$ is grouped into the eigenvalue λ.

Solution procedure

Step I. In order to match the standard form of generalized eigenvalue problem, multiply -1 on both sides of $\mathbf{B}\widehat{\phi} = -\lambda\mathbf{L}\widehat{\phi}$ and denote $\mathbf{B}' = -\mathbf{B}$. The new generalized eigenequation is therefore $\mathbf{B}'\widehat{\phi} = \lambda\mathbf{L}\widehat{\phi}$.

Step II. Compute the split Cholesky factorization of a real symmetric positive definite matrix $\mathbf{L}$ and record its factor matrix $\mathbf{S}$, $\mathbf{L} = \mathbf{S}^T\mathbf{S}$. In order to save storage memory, we use the band matrix form to present the sparse matrix $\mathbf{L}$ and the factor $\mathbf{S}$ is also returned in the band matrix form with the same bandwidth as $\mathbf{L}$. This step is implemented by the DPBSTF routine provided by LAPACK [2].

Step III. Following Step II the generalized eigenequation has been transformed to $\mathbf{B}'\hat{\phi} = \lambda\mathbf{S}^T\mathbf{S}\hat{\phi}$. Multiply $\mathbf{S}^{-T}$ on both sides; then we have

$$\mathbf{S}^{-T}\mathbf{B}'\mathbf{S}^{-1}\mathbf{S}\hat{\phi} = \lambda\mathbf{S}\hat{\phi}, \tag{A6}$$

where the identity matrix $\mathbf{I} = \mathbf{S}^{-1}\mathbf{S}$ is inserted to make the coefficient matrix $\mathbf{S}^{-T}\mathbf{B}'\mathbf{S}^{-1}$ on the left-hand side (LHS) symmetric. Generally $\mathbf{S}^{-T}\mathbf{B}'\mathbf{S}^{-1}$ is not a sparse matrix which will make the subsequent computation less effective. To solve this problem, we perform a similarity transformation by introducing an orthogonal matrix $\boldsymbol{Q}_1$:

$$\mathbf{Q}_1^T\mathbf{S}^{-T}\mathbf{B}'\mathbf{S}^{-1}\mathbf{Q}_1\mathbf{Q}_1^T\mathbf{S}\hat{\phi} = \lambda\mathbf{Q}_1^T\mathbf{S}\hat{\phi}, \tag{A7}$$

where we denote $\mathbf{C} = \mathbf{Q}_1^T\mathbf{S}^{-T}\mathbf{B}'\mathbf{S}^{-1}\mathbf{Q}_1$ and $\hat{y} = \mathbf{Q}_1^T\mathbf{S}\hat{\phi}$. Here $\mathbf{Q}_1$ is chosen to preserve the bandwidth of the matrix $\mathbf{B}$. This procedure is implemented by the DSBGST routine provided by LAPACK.

Step IV. The matrix $\mathbf{Q}_2$ is introduced to further transform $\mathbf{C}$ to a tridiagonal matrix:

$$\mathbf{Q}_2^T\mathbf{C}\mathbf{Q}_2 = \mathbf{C}', \tag{A8}$$

where $\mathbf{I} = \mathbf{Q}_2^T\mathbf{Q}_2$. This procedure uses a sequence of elementary reflections to transform the matrix $\mathbf{C}$. The transformations are applied to the matrix both from the right and from the left, preserving the matrix symmetry on each stage and sequentially removing nondiagonal elements. Numerically, this procedure is implemented by the DSBTRD routine provided by LAPACK.

Step V. After Step IV, Eq. (A7) becomes

$$\mathbf{C}'\hat{y}' = \lambda\hat{y}', \tag{A9}$$

where $\hat{y}' = \mathbf{Q}_2^T\hat{y}$. This is a standard eigenvalue problem. The eigenvalues λ can be calculated according to the increasing magnitude, and the corresponding eigenvectors $\{\hat{y}'_n\}$ are fulfilled by the DSTEVR subroutine provided by LAPACK.

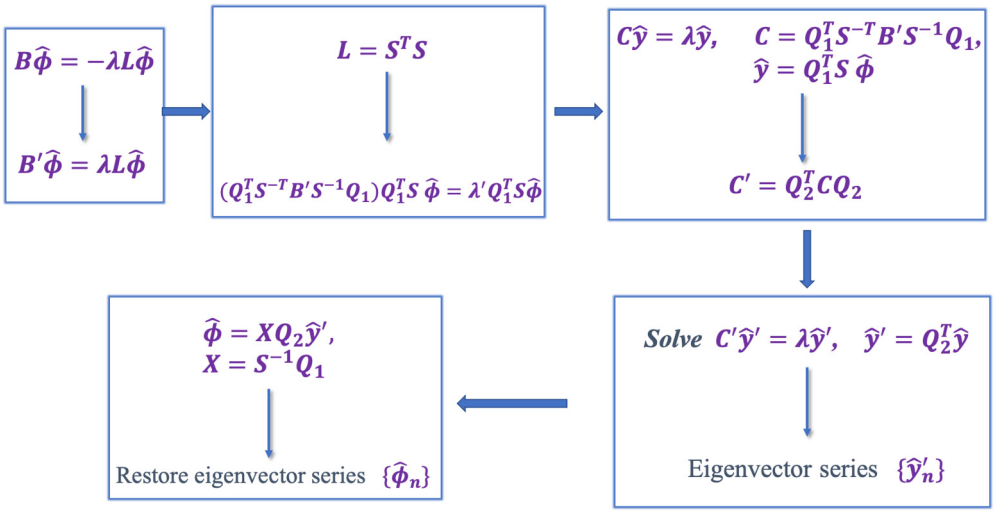

FIG. 7. A schematic flow chart for the solution procedure. The main purpose is to transform the required eigenvector $\hat{\phi}$ to the intermediate variable $\hat{y}'$, which satisfies $\hat{\phi} = S^{-1}Q_1Q_2\hat{y}'$. After obtaining the eigenvectors $\{\hat{y}_n'\}$, we retrieve the original scalar potential eigenvectors $\{\hat{\phi}_n\}$ through a linear transformation.

Step VI. Since the above transformations do not change the eigenvalues, we only need to restore the original eigenvectors. Combining all the above linear transformations we have

$$\hat{\phi} = \mathbf{S}^{-1}\mathbf{Q}_1\mathbf{Q}_2\hat{y}', \tag{A10}$$

where the intermediate coefficient matrix $\mathbf{X} = \mathbf{S}^{-1}\mathbf{Q}_1$ and $\mathbf{Q}_2$ need to be saved during the calculation.

APPENDIX B

In this Appendix we present the implementation details of MD simulation with the modulated slip boundary condition. Molecular dynamics simulations of the Lennard-Jones (LJ) potential fluid [16] confined between two parallel solid walls are carried out to numerically verify the spatial correlations induced by phase lock of HMs. There are two types of atoms in the MD system: fluid atoms and solid wall atoms. Here we choose the length unit $\sigma = 0.34$ nm, energy unit $\varepsilon = 0.997$ kJ/mol, and mass unit $m = 1.660 \times 10^{-27}$ kg as reduced units of measurement.

The solid wall has three layers of atoms arranged in a face centered cubic (fcc) lattice, and the modulation of the boundary condition is achieved by interlacing two types of solid atoms in a piecewise manner along the wall. Both wall atoms interact with the fluid atoms via the LJ potential $u_{ij}(\vec{r}) = 4\varepsilon_{ij}[(\sigma_{ij}/r)^{12} - \delta_{ij}(\sigma_{ij}/r)^6]$ where i, j refer to the either the fluid or the wall atom. Here "solid" is denoted by subscript w and "fluid" by subscript f. The solid wall atoms and fluid atoms are coupled to separate thermostats with different temperatures. Here the degree of freedom of the solid wall atoms is frozen for simplicity. Periodic boundary conditions were applied along all three directions with the periodicity along the y axis being as short as 2.176 nm (6.4σ). The reason for this choice is due to the requirement that the periodicity must be at least twice as larger as the cutoff radius $\sigma_c = 2.53\sigma$ of the LJ potential. Here we set $\varepsilon_{wf} = 1.16\varepsilon$, $\sigma_{wf} = 1.04\sigma$, and $\varepsilon_{ff} = \varepsilon$, $\sigma_{ff} = \sigma$, $\delta_{ff} = 1$. The two different solid-fluid intermolecular potentials are distinguished by parameters $\delta_{wf}^{(k)}$, $k = 1, 2$. The average number density of the fluid is set at $\rho = 0.824/\sigma^3$. To keep the MD system at a constant temperature equilibrium state we use the Nosé-Hoover chain algorithm [16,20,28] with chain length $l_c = 2$ as the fluid atoms' thermostat. The default time unit in GROMACS [19] is 1 ps and throughout the MD simulation the equations of motion are integrated with time a step of $\Delta t = 0.0001$ ps. Center of mass motion was removed at a frequency of 10 000 steps. We save the coordinates and velocity data to the trajectory file every 50 time steps.

We perform MD simulations at *NVT* ensemble constraints; i.e., the number of atoms, volume, and temperature of the system are all fixed. At the initial time step all fluid atoms were put at evenly distributed lattice sites with appropriate intervals. Then we added three layers of solid atoms arranged with face centered cubic structure both above and beneath the inserted fluid atoms. The geometric size of the channel is $2L \times 2H \times 2W$ with $2H = 16\sigma$, $2L = 64\sigma$, $2W = 6.4\sigma$. Here H denotes the fluid-solid interface in the MD configuration rather than the hydrodynamic boundary position h [9]. We evolve a total of 3 000 000 time steps starting from the initial configuration in order to attain the equilibrium state.

Before carrying out simulations of the microfluid system with the modulated boundary condition, we need to first perform MD simulations with the uniform boundary condition, i.e., constant slip length, in order to obtain the necessary slip length to be used in the HM calculations. By carrying out two such simulations, each with a different wall-fluid interaction potential, we can obtain two different slip lengths. These slip length values are the ones used in the HM calculations with the modulated slip boundary condition. The two different wall-fluid interaction potential values are also implemented in the MD simulation as interlaced periodic wall-fluid interaction potential as shown in Fig. 1 in the main text.

For the uniform slip boundary condition, analytic solution of the HMs can be obtained [1]. We use this analytic form

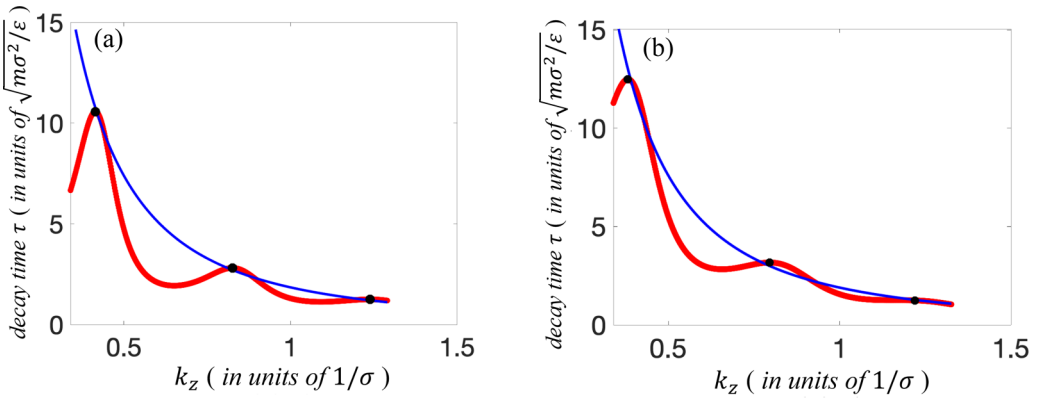

FIG. 8. Decay time τ plotted as a function of k_z in the uniform hydrodynamic boundary case. (a) For $\delta_{wf} = 1.2$, three black dots correspond to the peak points of the red curves, which theoretically predict the hydrodynamic modes' eigen wave vector k_z as well as its decay time. The upper blue curve corresponds to the relation $\tau k_z^2 = \rho/\eta$, where the viscosity $\eta = 0.445\sqrt{\varepsilon m}/\sigma^2$. (b) For $\delta_{wf} = 0.2$, three black dots correspond to the peak points of the red curves in reduced units.

of the HMs, with constant slip length, for projection onto the MD trajectories with specified $\delta_{wf}^{(k)}$, $k = 1, 2$ so as to obtain a mapping relation between the MD parameters and the slip length l_s, shown in Table I in the main text. This is achieved by applying the eigenmode projection method [1], i.e., plotting the decay time τ as function of k_z in which the decay time is defined as the inverse of the slope of the logarithm of the transverse momentum autocorrelation function $C_\beta(k_z, \Delta t)$, so that when the k_z value actually meets the boundary condition requirement in MD simulations, the corresponding decay time τ is expected to be a local maximum. In this manner, we can select at least three k_z values indicated by the peaks of the $\tau \sim k_z$ curve and calculate the cross products of velocity eigenmodes for any two of them to observe their first zero crossing as the hydrodynamic boundary position $h^{(k)}$. Once $h^{(k)}$ is determined, the corresponding slip length $l_s^{(k)}$ can be uniquely determined by solving the dispersion relation $\tan(k_z^{(n)}h) = -k_z^{(n)}l_s$. In this context we will briefly describe how to obtain the hydrodynamic parameters pair $(h^{(k)}, l_s^{(k)})$ for $\delta_{wf} = 1.2,\ 0.2$, respectively. More details of such procedure can be found in Refs. [1,9].

1. Case I. $\delta_{wf} = 1.2$

We project the one-dimensional HM with input series values of k_z onto the MD simulation trajectory with $\delta_{wf} = 1.2$ and evaluate its transverse momentum autocorrelation function $C_\beta(k_z, \Delta t)$,

$$C_\beta(k_z, \Delta t) = \frac{\left\langle \left(\sum_i^N \vec{v}[\vec{r}_i(t_0)] \cdot \vec{u}_\beta[\vec{r}_i(t_0)]\right)\left\{\sum_i^N \vec{v}[\vec{r}_i(t_0 + \Delta t)] \cdot \vec{u}_\beta[\vec{r}_i(t_0 + \Delta t)]\right\}\right\rangle}{\left\langle \left(\sum_i^N \vec{v}[\vec{r}_i(t_0)] \cdot \vec{u}_\beta[\vec{r}_i(t_0)]\right)\left\{\sum_i^N \vec{v}[\vec{r}_i(t_0)] \cdot \vec{u}_\beta[\vec{r}_i(t_0)]\right\}\right\rangle}. \tag{B1}$$

By taking the inverse of the slope of $\ln C_\beta(k_z, \Delta t)$, we obtain the plot of decay time τ as a function of Δt, shown in Fig. 3(a). The reason of choosing the one-dimensional (1D) mode [1,9] with $k_x = 0$ is that for the $k_x \neq 0$ case, *a priori* knowledge of hydrodynamic boundary position h is necessary in the calculation of $C_\beta(k_z, \Delta t)$. After selecting the k_z values of peak points of the $\tau \sim k_z$ curve, through invoking the relation $\tau k_z^2 = \rho/\eta$, the fluid viscosity η could be simultaneously determined, here $\eta = 0.445\ \sqrt{\varepsilon m}/\sigma^2$. In order to determine the hydrodynamic boundary position h, by invoking the mutual orthogonality of HMs we select three modes with k_z values indicated by the three black dots in Fig. 8(a), and integrate the cross products of any two of them from $z = 0$ towards the solid-fluid interface, denoted as 12, 13, and 23. If the continuous hydrodynamic equations are assumed to be correct, then the integration of these three cross products must vanish at the same location. This value of z is denoted as the hydrodynamic boundary position h. Once h is determined, the slip length l_s can be simultaneously calculated by substituting the eigenvectors $k_z^{(n)}$ and h into the dispersion relationships $\tan(k_z^{(n)}h) = -k_z^{(n)}l_s$. When $\delta_{wf} = 1.2$, the hydrodynamic parameters are $h = 7.5\sigma$ and $l_s = 0.1\sigma$.

2. Case II. $\delta_{wf} = 0.2$

Following the same procedures with case I, we plot the decay time τ as a function of time Δt, shown in Fig. 8(b). The first three peaks of k_z values as well as its corresponding decay time τ are selected as HMs satisfying the boundary conditions. When $\delta_{wf} = 0.2$, the hydrodynamic parameters are $h = 6.8\sigma$ and $l_s = 1.5\sigma$.

It is to be noted that there is a very small difference in the positions of the hydrodynamic boundary for the two cases. This small difference is ignored in our continuum calculations.

[1] X. H. Deng, X. Y. Wei, X. P. Wang, and P. Sheng, Phys. Rev. E **101**, 063104 (2020).

[2] E. Anderson, Z. Bai, C. Bischof, S. Blackford, J. Demmel, J. Dongarra, J. Du Croz, A. Greenbaum, S. Hammarling, A. McKenney, and D. Sorensen, *LAPACK Users' Guide*, 3rd ed. (SIAM, Philadelphia, 1999).

[3] G. Guennebaud and B. Jacob, EIGEN, http://eigen.tuxfamily.org

[4] See Appendix A for a numerical scheme for obtaining the hydrodynamic eigenfunctions under the modulated slip boundary condition, and Appendix B for implementation details of MD simulation with the modulated slip boundary condition.

[5] P. Joseph and P. Tabeling, Phys. Rev. E **71**, 035303(R) (2005).

[6] A. E. Kobryn and A. Kovalenko, J. Chem. Phys. **129**, 134701 (2008).

[7] L. Bocquet and J. L. Barrat, Soft Matter **3**, 685 (2007).

[8] M. Cieplak, J. Koplik, and J. R. Banavar, Phys. Rev. Lett. **86**, 803 (2001).

[9] S. Chen, H. Wang, T. Qian, and P. Sheng, Phys. Rev. E **92**, 043007 (2015).

[10] L. Bocquet and J. L. Barrat, Phys. Rev. E **49**, 3079 (1994).

[11] L. Bocquet and J. L. Barrat, Phys. Rev. Lett. **70**, 2726 (1993).

[12] L. Bocquet and J. L. Barrat, J. Chem. Phys. **139**, 044704 (2013).

[13] P. A. Thompson and S. M. Troian, Nature **389**, 360 (1997).

[14] T. Qian, X. P. Wang, and P. Sheng, J. Fluid Mech. **564**, 333 (2006).

[15] K. Meier, A. Laesecke, and S. Kabelac, J. Chem. Phys. **121**, 3671 (2004).

[16] D. Frenkel and B. Smit, *Understanding Molecular Simulation from Algorithms to Applications*, 2nd ed. (Academic Press, San Diego, 2002).

[17] J. Petravic and P. Harrowell, J. Chem. Phys. **124**, 014103 (2006).

[18] J. Petravic and P. Harrowell, J. Chem. Phys. **127**, 174706 (2007).

[19] M. J. Abraham, D. van der Spoel, E. Lindahl, B. Hess, and the GROMACS development team, *GROMACS User Manual*, version 2019, http://www.gromacs.org/.

[20] G. J. Martyna and M. L. Klein, J. Chem. Phys. **97**, 2635 (1992).

[21] K. Huang, *Statistical Mechanics*, 2nd ed. (Wiley, New York, 1987).

[22] L. D. Landau and E. M. Lifshitz, *Statistical Physics. Part 1*, 3rd ed., Course of Theoretical Physics Vol. 5 (Elsevier, Amsterdam, 1980).

[23] F. Detcheverry and L. Bocquet, Phys. Rev. Lett. **109**, 024501 (2012).

[24] D. J. Evans and G. Morriss, *Statistical Mechanics of Nonequilibrium Liquids*, 2nd ed. (Cambridge University Press, Cambridge, 2008).

[25] R. Kubo, Rep. Prog. Phys. **29**, 255 (1966).

[26] R. Kubo, J. Phys. Soc. Jpn. **12**, 570 (1957).

[27] B. M. A. Hamed, M. H. A. Hashim, M. A. Ahmed, S. K. Manju Bargavi, and S. Ranjith Kumar, Int. J. Adv. Comput. Sci. Technol. **2**, 111 (2013).

[28] M. Allen and D. Tildesley, *Computer Simulation of Liquids* (Oxford University Press, Oxford, 1987).